Appl. Phys. A (2016) 122:686
DOI 10.1007/s00339-016-0194-5

Applied Physics A
Materials Science & Processing

Synthesis of superhydrophobic ultralight aerogels from nanofibrillated cellulose isolated from natural reed for high-performance adsorbents

Yue Jiao[1] · Caichao Wan[1] · Tiangang Qiang[1] · Jian Li[1]

Received: 24 February 2016 / Accepted: 6 June 2016 / Published online: 21 June 2016

Abstract Reed is one of the widely available aquatic plant resources, and its applications are generally limited to some traditional areas like papermaking and animals' fodder. Besides, most of reed is wasted or directly burned every year causing serious air pollution (like atmospheric haze). Therefore, it is worth to further develop new forms of high-value applications of reed. Herein, natural reed was collected to fabricate ultralight adsorbents namely nanofibrillated cellulose (NFC) aerogels via an easily operated method, which includes chemical purification, ultrasonication, and freeze drying. The NFC aerogels with an ultra-low density of 4.9 mg cm^{-3} were characterized by scanning electron microscopy, energy-dispersive X-ray spectrometer, Fourier transform infrared spectroscopy, X-ray diffraction, and thermogravimetric analysis. For acquiring good hydrophobicity, the NFC aerogels were subjected to a hydrophobic treatment by methyltrichlorosilane. The superhydrophobic NFC aerogels with contact angles of as high as 151°–155° have excellent adsorption efficiency (53–93 g g^{-1}) for various organic solvents and waste oil. More importantly, the aerogels also exhibit favorable adsorption recyclability, which can maintain more than 80 % of the initial adsorption efficiency after the five cycles.

1 Introduction

With the rapid consumption of oil resource day by day, it is necessary to use green, economic, and renewable resources to exploit new materials to substitute for traditional petrochemical products. Cellulose is one of the most abundant reproducible natural polymers on earth. Especially, the individual cellulose nanofibrils have gained increasing attentions. Besides their nanosize dimensions, cellulose nanofibrils have other advantages like outstanding mechanical properties, low density, biocompatibility, and high reactivity [1, 2]. As a result, cellulose nanofibrils can be useful in various fields, such as reinforcement components in flexible display panels [3], biodegradable packaging materials [4], and oxygen-barrier layers [5]. In recent decades, several techniques have been proposed to extract highly purified nanofibrils from various cellulosic resources, such as high pressure homogenization [6], high-speed shearing [7], and TEMPO-mediated oxidation combined with mechanical treatment [8]. All these methods can obtain different types of nanofibrils, primarily depending on both raw materials and disintegration process. Among the existent approaches, ultrasonic technique has been extensively examined for materials synthesis and considered as one of the most powerful tools to isolate cellulose

Yue Jiao and Caichao Wan have contributed equally to this work and are considered co-first authors.

Electronic supplementary material The online version of this article (doi:10.1007/s00339-016-0194-5) contains supplementary material, which is available to authorized users.

✉ Tiangang Qiang
neduxgb@126.com

✉ Jian Li
lijiangroup@163.com

Yue Jiao
yjiao123@126.com

Caichao Wan
wancaichaojy@163.com

[1] Material Science and Engineering College, Northeast Forestry University, No. 26, Hexing Road Xiangfang District, Harbin 150040, People's Republic of China

nanofibrils [9, 10]. Such powerful ultrasonic environments provide a unique platform to break the firm hydrogen bonding between nanofibrils, allowing individual nanofibrils to be gradually separated. Apart from the remarkable merits, it is also worth to mention that the ultrasonication causes cellulose degradation to some extent. To date, the effect of ultrasonication in degrading polysaccharide linkages has been well described [11–13].

Reed is a kind of annual herb plant which is distributed in temperate and tropical zone. It mainly grows in irrigation canals, river near swamps, etc. Reed is composed of about 49.4 % cellulose, 31.5 % hemicellulose, 8.8 % lignin, and other substrates [14]. The applications of reed are generally limited to some traditional areas like papermaking and animals' fodder. Besides, most of reed is wasted or burned every year. Therefore, it is important to further develop new forms of high-value application of this resource. The cell walls of plant usually consist of rigid cellulose microfibrils embedding in the soft hemicellulose and lignin matrix [15, 16]. Cellulose microfibrils consist of numerous cellulose nanofibrils which are tightly hooked to one another by multiple hydrogen bonds. Thus, it is difficult to split cellulose nanofibrils only by mechanical treatments. Many researchers [17, 18] reported that the matrix substances can be removed using chemical methods before the fibrillation process. As a result, the narrow cellulose nanofibrils can be obtained by the combination of chemical treatment and ultrasonication. More interestingly, a class of aerogels can be prepared from the aqueous or alcohol dispersion of cellulose nanofibrils using freeze-drying technique. Pääkkö et al. [19] firstly reported cellulose I nanofiber aerogels with a specific surface area of 66 $m^2\ g^{-1}$, which was fabricated by freeze-drying treatment of NFC dispersion. Sehaqui et al. [20] then prepared nanofibrillated cellulose (NFC) aerogels with high specific surface area (153–284 $m^2\ g^{-1}$), high porosity (93–99 %), and low density (14–105 mg cm^{-3}) via the multiple-stage solvent exchange technique followed by freeze drying. Also, the NFC aerogels were used as templates to combine with hydrophobic silanes [21], Fe_3O_4/Ag [22], polypyrrole [23], and *N*-(2-aminoethyl)-3-aminopropylmethyldimethoxysilane [24] for some advanced applications including oil–water separation, catalyst, antibacterial agent, CO_2 capture from air, and electrochemical devices. It is well-known that silica aerogels [25, 26] and carbon aerogels (typically like carbon nanofiber aerogels [27, 28], all-carbon aerogels containing graphene sheets and carbon nanotubes [29], and carbon aerogels from the carbonization of organic aerogels [30]) have been extensively used as absorbent materials to treat with organic pollutants. However, there are not plentiful reports focusing on the adsorption property of biodegradable NFC aerogels for toxic organic liquids and their adsorption recyclability. Therefore, it is desirable to carry out these researches.

In this study, we used waste natural reed as raw material to fabricate ultralight NFC aerogels following the procedures of chemical purification, ultrasonication, and freeze drying. Compared with the commercially available cellulosic feedstocks such as wood pulp and dissolving pulp, reed is cheaper and widely available. Moreover, the utilization of reed is consistent with our objective of achieving high-value utilization of low-value bioresources. The effects of the chemical purification and ultrasonication on the morphology, chemical composition, crystal structure, and thermal stability were investigated. After the modification by methyltrichlorosilane (MTCS), the aerogels acquired superhydrophobicity with contact angles of as high as 151°–155°. In addition, their adsorption efficiency for various common organic solvents and waste oil can reach up to 53–93 g g^{-1}. For measuring their adsorption recyclability, we put the aerogels into a thin and lightweight nonwoven cloth bag considering the poor mechanical property of the aerogels, and the bag filled with the samples were dipped into various organic liquids. Two simple methods (i.e., squeezing–vacuum drying and air drying) were used to separate the liquids from the bag, dependent on the type of pollutants. The results show that the adsorbent can maintain more than 80 % of the initial adsorption efficiency after the five cycles. These make the aerogels alternative biodegradable adsorbents to treat with organic pollutants.

2 Experimental

2.1 Materials

The reed powder was sieved through a 60 mesh screen and used as the raw material. All the chemicals including benzene, ethanol, sodium chlorite, potassium hydroxide, hydrochloric acid (37 %), and tert-butyl alcohol were analytically pure, supplied by Tianjin Kermel Chemical Reagent Co. Ltd. (China) and used without further purification.

2.2 Separation of NFCs from reed

The separation process involves chemical purification and ultrasonication [31, 32]. For the chemical purification, the dried reed powder (2 g) was firstly extracted with benzene/ethanol (2:1, v:v) in soxhlet at 90 °C for 24 h to remove pectin and waxes and then dried in an oven for 24 h at 50 °C. Secondly, lignin was removed by mixing the resulting sample with acidified sodium chlorite solution at 75 °C for an hour. This process was repeated five times. Thirdly, hemicellulose was removed by an alkaline treatment (2 wt% potassium hydroxide solution) at 90 °C for

2 h. Finally, the samples were treated with the hydrochloric acid (1 wt%) at 80 °C for 2 h, and subsequently filtered and rinsed with a large amount of distilled water. The purified cellulose was dried at 50 °C to constant weight. The yield of cellulose is around 22.5 %, which was roughly calculated by dividing the product dry weight by the weight of the dried reed powder.

For the ultrasonication process, the purified cellulose was firstly dispersed in distilled water to form a 0.05 wt% aqueous suspension (300 mL), and the suspension was then placed into an ultrasonic generator. Sonication was performed at 20–25 kHz with a sonifier cell disruptor (JY99-IID, Scientz Technology, China) with a 1-cm^2-diameter titanium horn under a 50 % duty cycle (i.e., a repeating cycle of 0.5 s ultrasonic treatment and 0.5 s shutdown). The sonication was conducted for 1 h with an output power of 900 W in an ice/water bath. After that, the NFC suspension was obtained.

2.3 Preparation of NFC aerogels

The NFC suspension was subjected to a solvent exchange with tertiary butanol by dipping the dialysis tubing containing the suspension into tertiary butanol until the volume of the suspension was reduced to approximately one-fifth. The concentrated NFC suspension was collected and poured into molds and then freeze-dried to sublimate tertiary butanol directly from solid phase to gas phase. The cold trap temperature and pressure are around −55 °C and 25 Pa during the whole freeze-drying process.

2.4 Hydrophobic treatment of NFC aerogels

The hydrophobic NFC aerogels were obtained by the treatment of MTCS through the vapor phase deposition. In a typical process, the aerogels were placed in a glass desiccator, and a small glass vial containing 300 μL MTCS was then added into the desiccator. The desiccator was sealed, and the samples and the reagent were allowed to react at room temperature for 24 h.

2.5 Characterizations

The morphology was characterized by scanning electron microscopy (SEM, FEI Sirion 3030) operating at 15.0 kV. Elemental analysis was conducted by an energy-dispersive X-ray (EDX) spectrometer. Fourier transform infrared (FTIR) spectra were recorded on a FTIR instrument (Nicolet 6700, Thermo Fisher Scientific., USA) in the range of 400–4000 cm^{-1} with a resolution of 4 cm^{-1}. The crystal structures were characterized via X-ray diffraction (XRD, Rigaku D/MAX 2200) operating with Cu Ka radiation ($\lambda = 1.5418$Å) at a scan rate (2θ) of 4 min^{-1} ranging from 5° to 40°. Thermogravimetric analysis (TGA) was performed with a synchronous thermal analyser (TA, Q600) from room temperature to 800 °C at a heating rate of 10 °C min^{-1} under a nitrogen atmosphere. The surface wettability was evaluated by contact angle measurement, using a Powereach JC2000C contact angle analyser. N_2 adsorption–desorption measurements were implemented at −196 °C using an accelerated surface area and porosimetry system (3H-2000PS2 unit, Beishide Instrument S&T Co. Ltd.). The specific surface area was calculated over a relative pressure range of 0.05–0.30 from the multipoint Brunauer—Emmett—Teller (BET) method. The nitrogen adsorption volume at the relative pressure (P/P_0) of 0.99 was used to determine the pore volume. The pore diameter distributions were calculated from the data of the adsorption branch of the isotherm using the Barrett—Joyner—Halenda (BJH) method.

2.6 Adsorption tests for various organic liquids

The adsorption tests were conducted by dipping the MTCS-treated NFC aerogels into various organic liquids for 1 min. The sample weight was measured before and after the tests. The adsorption property was characterized by adsorption efficiency, which was calculated by dividing the wet weight of the sample after the adsorption tests by the initial weight.

2.7 Cyclic adsorption tests

We firstly put the MTCS-treated NFC aerogels (ca. 0.05 g) into a thin and lightweight nonwoven cloth bag (6 cm × 8 cm, 0.25–0.35 g). Then the bag was sealed and dipped into methylbenzene (or ethyl alcohol) for 1 min. The adsorbed methylbenzene (or ethyl alcohol) was separated from the adsorbent by squeezing–vacuum drying (or air drying). The adsorption–desorption process was repeated five times. The weight of the bag was measured before and after each period.

3 Results and discussion

3.1 Morphology observation and elemental analysis

The SEM images of the reed, purified cellulose, and NFC aerogels are presented in Fig. 1a–c. As shown in Fig. 1a, the microstructure of reed outer epidermis is provided, and a plenty of pits can be clearly seen. Besides, according to the EDX analysis (Fig. 1d), the elements including C, O, Si, Cl, K and Na were detected for the reed, and the corresponding proportions are 54.64, 25.33, 17.49, 0.91, 0.88, and 0.75 wt%, respectively. The Au element is originated

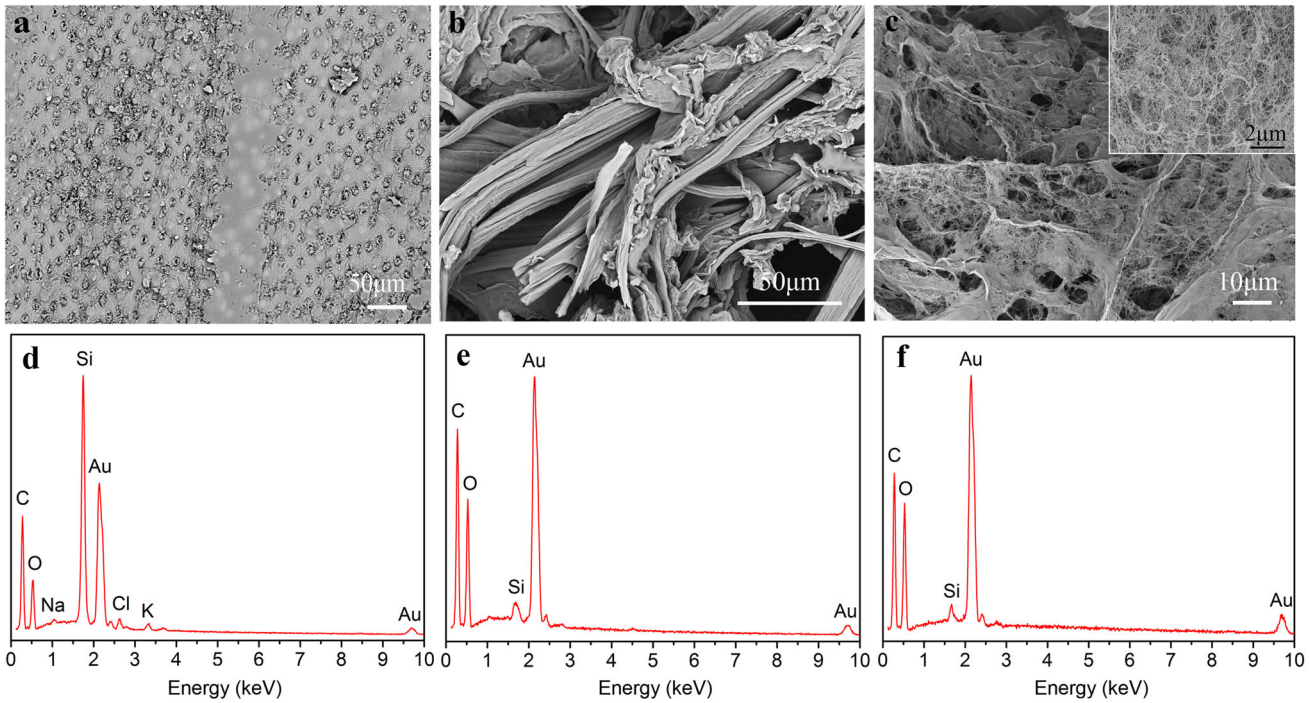

Fig. 1 **a–c** SEM images of the reed, purified cellulose, and NFC aerogels, respectively. *Inset* of (**c**) is the corresponding enlarged image. **d–f** present the EDX spectra of the reed, purified cellulose, and NFC aerogels, respectively

from the coating layer used for electric conduction during the SEM observation. Through the removal of non-cellulosic substances (such as waxes, pectin, hemicellulose, and lignin) by the purification, it can be seen that the macrofibrils composed of a bundle of microfibrils are disintegrated [33], and the numerous microfibrils were successfully isolated (Fig. 1b). In addition, from the EDX spectrum in Fig. 1e, there are only three elements here (i.e., C, O and Si), which indicates that the most mineral substances had been removed by the chemical purification.

As mentioned above, cellulose microfibrils are composed of numerous tightly connected cellulose nanofibrils which are hard to be split. Ultrasonication can provide local hot spots with high temperature and pressure as well as rapid heating/cooling rate, which can effectively destroy the intermolecular hydrogen bonding between the linear polymers. Although ultrasonication is a powerful tool to isolate cellulose nanofibrils, ultrasonication causes cellulose degradation. Sonication of cellulose in aqueous suspension leads to the depolymerization of cellulose. It is found that changes in the molecular structure of cellulose are attributed to the hydrolysis (chain cleavage) [11]. Figure 1c shows the morphology of NFC aerogels formed by the self-assemble of abundant NFCs. The cross-linked 3D network can be identified. Moreover, the inset of Fig. 1c confirms that the nanoscale NFCs were successfully separated. We drew the frequency distribution histogram of NFCs diameters (see Fig. S1 in the Supporting Information), and the plot exhibits a Gaussian-like distribution. The diameter of NFCs ranges from 10 to 37 nm, similar to that of some previously reported cellulose nanofibers obtained by ultrasonic method in literatures [34] (10–40 nm), [35] (30–100 nm), and [36] (2–50 nm). In addition, it can be found that the NFCs in our paper have narrower diameter distribution. Moreover, the average size (d) and standard deviation (σ) were calculated as 22.67 and 5.79 nm, respectively.

3.2 Chemical composition, crystal structure, and thermal stability

FTIR was carried out to clarify the differences in chemical compositions. The FTIR spectra of reed, purified cellulose, and NFC aerogels are presented in Fig. 2, and their main signals are illustrated in Table 1. For the reed, the absorption at 3329 cm^{-1} is attributed to the O–H stretching, and the bands at 2917 and 2850 cm^{-1} are attributed to C–H asymmetric and symmetric stretching vibrations [37], respectively. The bands at 1421, 1369, 1315, and 1234 cm^{-1} originate from CH_2 scissoring, C–H stretch in CH_3, CH_2 rocking vibration, and C–O–C stretching. The C–O–C pyranose ring skeletal vibration gives a prominent band at 1029 cm^{-1}. A small sharp peak at 891 cm^{-1} corresponds to the glycosidic C_1–H deformation with ring vibration contribution, which is characteristic of β-glycosidic linkages between glucose in cellulose [38]. The band

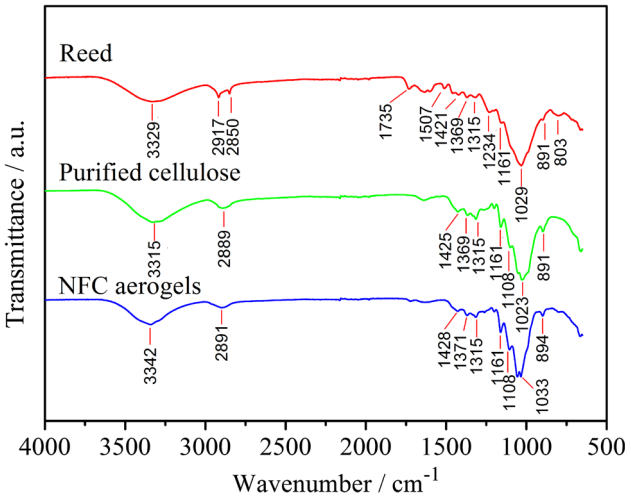

Fig. 2 FTIR spectra of the reed, purified cellulose, and NFC aerogels, respectively

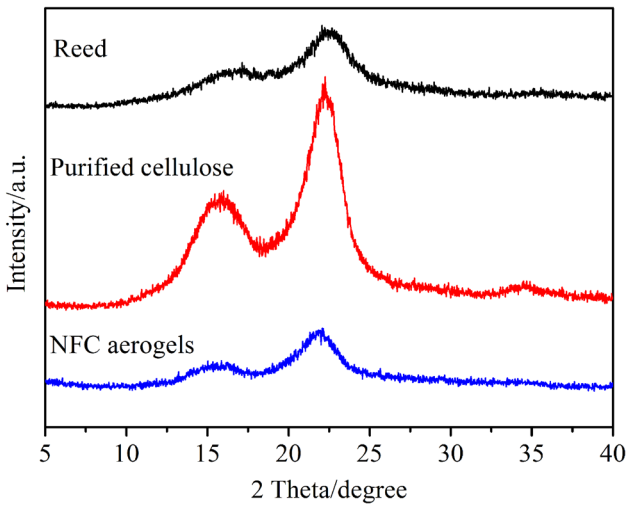

Fig. 3 X-ray diffraction patterns of the reed, purified cellulose, and NFC aerogels, respectively

at 803 cm^{-1} is due to pyran vibration. Compared with the spectrum of the reed, there are small differences in the spectra of purified cellulose and NFC aerogels. The peak at 1507 cm^{-1} attributed to aromatic skeletal vibrations of lignin [39] disappears completely after chemical purification. The outstanding peak at 1735 cm^{-1} also disappears, which is derived from either the acetyl and uronic ester groups of the hemicellulose or the ester linkage of the carboxylic groups of the ferulic and *p*-coumaric acids of lignin and/or hemicellulose [40]. Therefore, these results suggest that hemicellulose and lignin were effectively removed by the chemical purification. In addition, comparing the purified cellulose and the NFC aerogels, there is no remarkable difference in some bands (typically at 1421 and 897 cm^{-1}) sensitive to crystal form [41], which reveals that the ultrasonication did not change the cellulose crystal form.

For further investigating the changes in crystal structure, the XRD patterns of the reed, purified cellulose, and NFC aerogels are compared. In Fig. 3, we can see that all samples exhibit a sharp peak at around 22.3° from the (002) plane and a broad peak at around 16.5° due to the mixture of peaks from (101) and (10$\bar{1}$), corresponding to typical cellulose I crystal structure with parallel up arrangement of cellulose chains [42]. It indicates that the chemical purification and ultrasonication did not change the crystal form of cellulose. However, these treatments significantly affect the peak intensity, suggesting the probable variations in crystallinity. The crystallinity index (CrI) was calculated as the ratio of the area arising from the crystalline phase to the total area, and the fitting of XRD patterns is provided in Figure S2 (see Supporting Information). Compared to the reed, the crystallinity index of the purified cellulose increases by 8.81 % (from 58.61 to

Table 1 Frequencies (cm^{-1}) of the main signals of the reed, purified cellulose, and NFC aerogels, respectively

Absorption band (cm^{-1})	Assignment
3329	Valence vibration of hydrogen bonded OH-groups
2917–2850	CH_2 valence vibration
1735	C=O valence vibration of acetyl or COOH-groups
1507	Aromatic skeletal vibrations;
1421	CH_2 scissoring
1369	C–H stretch in CH_3
1315	CH_2 rocking vibration
1234	C–O–C stretching
1108	Ring asymmetric valence vibration
1029	C–O–C pyranose ring skeletal vibration
891	Anomer C-groups, C_1–H deformation, ring valence vibration
803	Pyran vibration

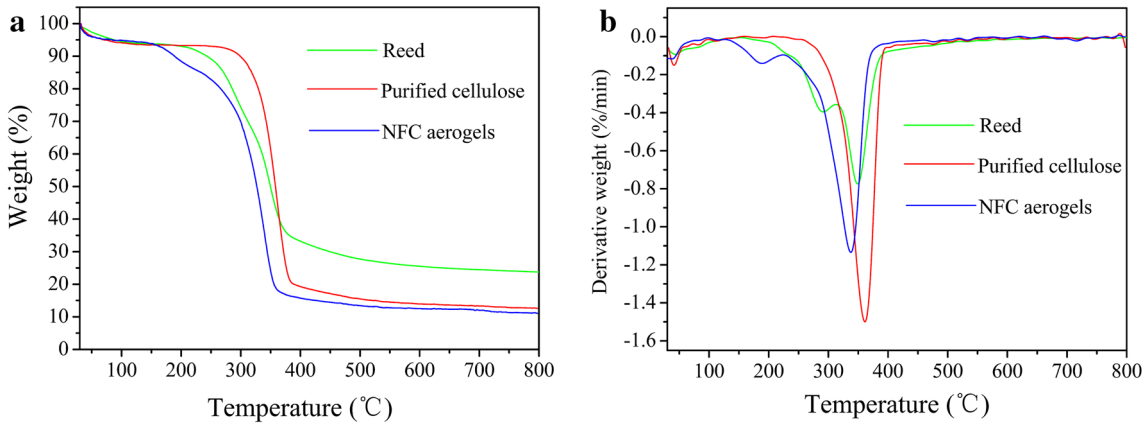

Fig. 4 **a** TGA and **b** DTG curves of the reed, purified cellulose, and NFC aerogels, respectively

67.42 %), due to the removal of hemicellulose and lignin which exist in the amorphous substances. Nevertheless, the crystallinity index of NFC aerogels (62.88 %) was 4.54 % lower than that of the cellulose. Li et al. [12] attributed the decrease in crystallinity index to the non-selective effect of ultrasonication, meaning that it can remove both amorphous and crystalline cellulose.

The thermal stability of the reed, purified cellulose, and NFC aerogels was studied by TGA and derivative thermogravimetry (DTG) in Fig. 4. The reed shows two main exothermic peaks. The former (200–310 °C) is mainly associated with the hemicellulose decomposition, which exhibits a pronounced shoulder [43]. The latter (310–400 °C) is principally assigned to cellulose degradation [44]. Owing to the wide decomposition temperature and slow decomposition rate of lignin, no characteristic peak related to lignin can be seen in the whole pyrolysis process [45]. In addition, it is worth to mention that cellulose decomposition is expressed by two competitive degradation reactions, one ascribed to the formation of tars (mainly levoglucosan) and char, the other to the light gases [46]. The formation of levoglucosan from cellulose pyrolysis has been proposed as the cleavage of the 1, 4-glycosidic linkage in the cellulose polymer followed by intramolecular rearrangement of the monomer units [47]. Recent literatures [48] confirm that the thermal decomposition of levoglucosan is extended over a wider temperature range (200–800 °C) according to the interaction of hemicellulose or lignin upon the pyrolysis of cellulose. Comparing the reed and the purified cellulose, it is not hard to see that the purified cellulose displays more superior thermal stability. The strongest peak of the cellulose is located at 361.7 and 15.3 °C higher than that of the reed (346.4 °C). The removal of amorphous substances contributes to this improvement. In addition, the fast heating rate and the different thermal conductivity of substances extracted from the reed possibly create a more remarkable heat transfer problem between the sample and the instrument [49], as compared to the purified cellulose. Thus, the maximum degradation rate of the reed might shift to a higher temperature. In contrast, the NFC aerogels have a poorer thermal stability, whose strongest peak is centered at 337.9 °C much lower than the others. It is well-known that crystallinity plays an important role in thermal properties of cellulose products [50]. Therefore, this decline can be explained by the damage of crystal structure by the ultrasonication.

3.3 Hydrophobic modification and adsorption property

After a series of treatments including chemical purification, ultrasonication, and freeze drying, we can obtain the ultralight NFC aerogels with an ultra-low bulk density of 4.9 mg cm^{-3}. Table 2 summarizes some lightweight cellulose aerogels. The density of the NFC aerogels reported in this paper is much higher than that reported by Chen et al. (0.2 mg cm^{-3}) [51], but comparable to or slightly lower than others [19, 20, 52–55]. Nowadays, lightweight materials have attracted great interests from numerous advanced areas, especially for adsorbing materials. Herein, as an example of potential application, the NFC aerogels were adopted as adsorbents to adsorb various organic solvents and waste oil. Prior to the adsorption, the aerogels were subjected to a facile hydrophobic modification by MTCS for enhancing the interfacial compatibility between hydrophilic cellulose and hydrophobic organic liquids. The hydrophobicity was evaluated by the contact angle measurement. It is obvious that the MTCS-treated aerogels have good hydrophobic property for various liquids (Fig. 5a), from up to down, including Coca-Cola, methyl orange, indigo carmine, rhodamine b, and milk. Figure 5b presents the corresponding images of contact angle tests. The untreated NFC aerogels show strong hydrophilicity,

Table 2 Bulk density of some lightweight cellulose aerogels

Materials	Feedstock	Method	Bulk density (mg/cm^3)	Reference
NFC aerogels	Dissolving pulp	Freeze drying	7–30	[52]
NFC aerogels	Hardwood	Freeze drying	9.8	[53]
NFC aerogels	Cellulose fibers	Supercritical drying	10–60	[54]
NFC aerogels	Wood pulp	Freeze drying	14–105	[20]
Bacterial cellulose aerogels	*Gluconacetobacter xylinum*	Supercritical drying	8	[55]
Cellulose I nanofibers aerogels	Softwood cellulose pulp	Freeze drying	20	[19]
Cellulose I nanofibers aerogels	Wood fibers	Freeze drying	0.2	[51]
NFC aerogels	Reed	Freeze drying	5	This work

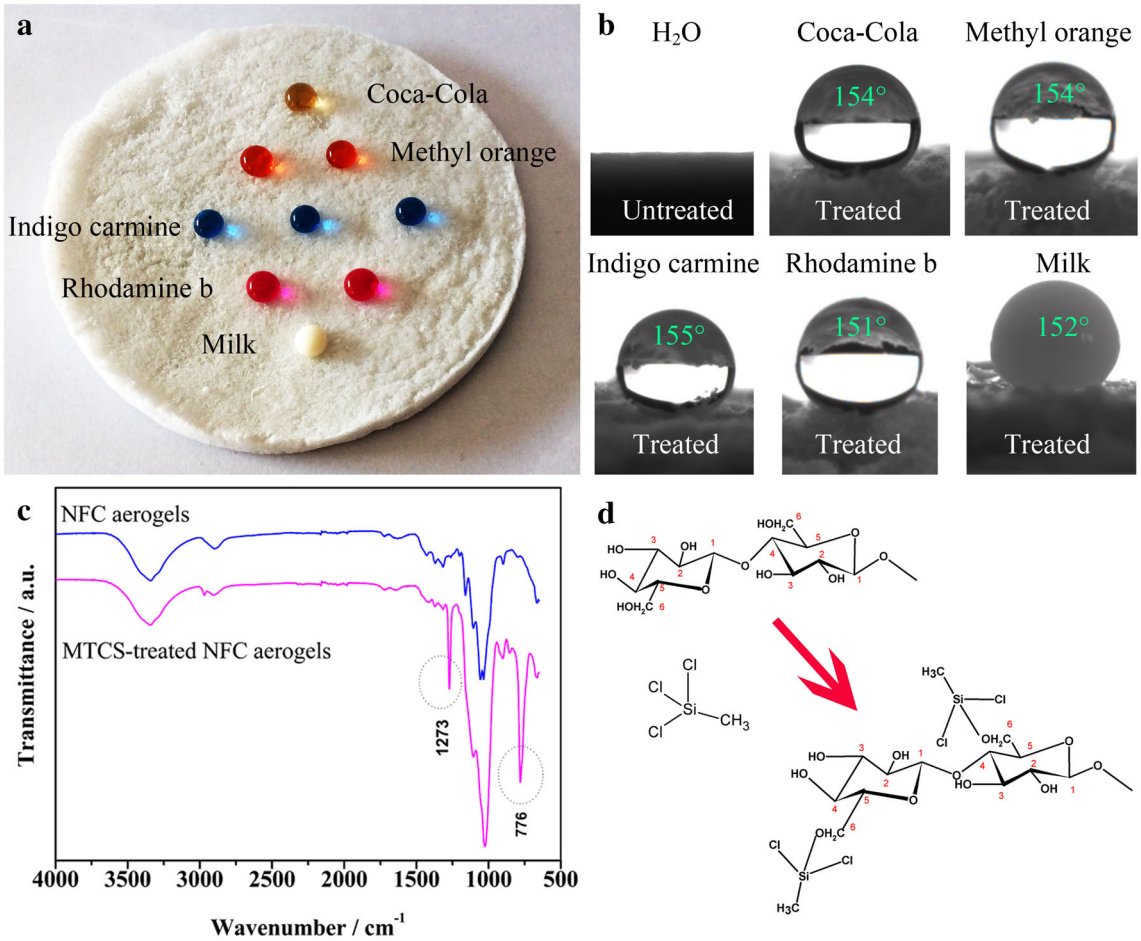

Fig. 5 **a** Liquid drops on the MTCS-treated NFC aerogels surface. **b** Contact angle measurements and **c** FTIR spectra of the untreated and MTCS-treated NFC aerogels. **d** Possible reaction mechanism between cellulose and MTCS

and cannot support water drop on the surface. After treated with MTCS, the aerogels acquired a high hydrophobicity and the contact angle values reach up to 151–155° for these liquids. The FTIR spectrum in Fig. 5c further confirms the formation of hydrophobicity for the treated aerogels. The two new strong peaks at around 1273 and 776 cm^{-1} are attributed to the stretching vibrations of the Si–C bonds and the –CH_3 deformation vibrations [56]. Moreover, the possible reaction mechanism between the cellulose and the reagent is given in Fig. 5c.

N_2 adsorption–desorption isotherms can provide much useful information about the pore structures of the MTCS-

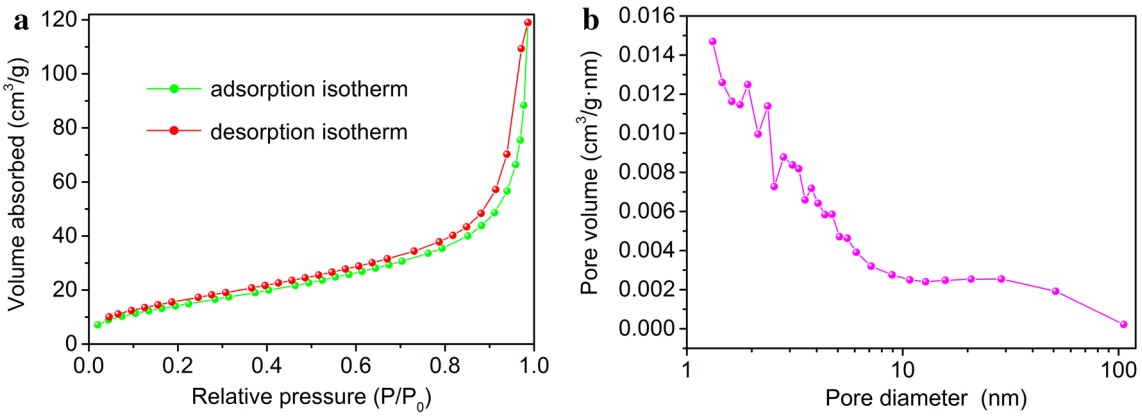

Fig. 6 **a** N_2 adsorption–desorption isotherms and **b** pore size distribution of the MTCS-treated NFC aerogels

treated NFC aerogels. As shown in Fig. 6a, the aerogels display an IV-type adsorption isotherm according to the IUPAC classification and the obvious hysteresis loop between the adsorption and desorption isotherms was originated from capillary condensation. Moreover, the pore size distribution shown in Fig. 6b exhibits that the pore sizes are within the scope of 1–106 nm, indicating the existence of micropores (<2 nm), mesopores (2–50 nm) and macropores (>50 nm). BET and BJH analyses give specific surface area and pore volume of 55.2 $m^2\ g^{-1}$ and 0.18 $m^3\ g^{-1}$ for the aerogels. The value of specific surface area is much lower than that reported by Sehaqui et al. [20] (249 $m^2\ g^{-1}$), but comparable to or even slightly higher than that in literatures [19] (66 $m^2\ g^{-1}$), [21] (42 $m^2\ g^{-1}$), [53] (18.4 $m^2\ g^{-1}$), and [52] (15 $m^2\ g^{-1}$). Moreover, the aerogels have a very high porosity, ca. 99.7 %, where the porosity Φ is defined as $\Phi = 1-(\rho/\rho_s)$, where ρ and ρ_s (1.5 g cm^{-3}) [21] are the bulk densities of the aerogel and the crystalline cellulose, respectively.

The wastewater of industry includes various organic pollutants like acetone, benzene, ethyl acetate, oleic acid, toluene and trichloromethane, and waste oil. It is meaningful to investigate the adsorption property of the MTCS-treated NFC aerogels for these organic pollutants. The adsorption results in Fig. 7 show that the adsorption efficiency of the MTCS-treated aerogels reaches up to 53–93 g g^{-1}. The adsorption efficiency for methylbenzene was taken as an example to make a comparison with other cellulose-based adsorbents reported elsewhere. The methylbenzene adsorption efficiency of the aerogels (ca. 92 g g^{-1}) in this work is slightly higher than that of the silylated nanocellulose sponges (ca. 62 g g^{-1}) [57] and the cellulose nanofibrils aerogels modified by styrene/acrylic monomers (ca. 30 g g^{-1}) [58]. Recently, Jiang and Hseih [59] achieved greater adsorption efficiency of methylbenzene (ca. 250 g g^{-1}) by vapor depositing triethoxyl (octyl)silane onto cellulose nanofibrils aerogels.

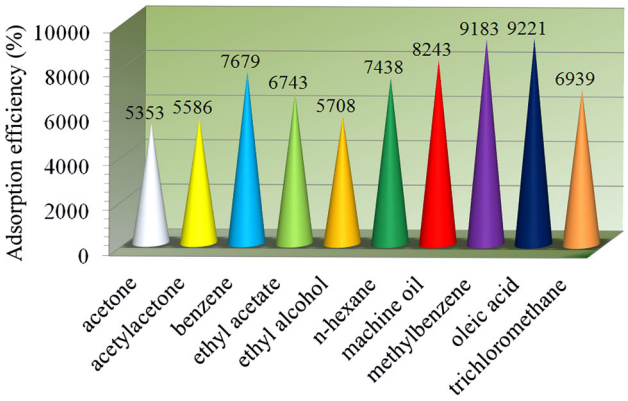

Fig. 7 Absorption efficiency of the MTCS-treated NFC aerogels for various organic solvents and waste machine oil

Besides substantial adsorption efficiency, adsorption recyclability is also of essential importance for ideal adsorbing materials. Good adsorption recyclability is beneficial to save costs, reduce energy consumption of preparation, and reduce generation of garbage. Considering some characteristics of the NFC aerogels adverse to the cyclic adsorption (e.g., poor mechanical property and strong shrinkage), the MTCS-treated NFC aerogels were put into a thin and lightweight nonwoven cloth bag. The bag was sealed and subjected to the cyclic adsorption tests. In this way, we need not worry about the shrinkage, operational and recycling problems. We adopted two methods to recycle the adsorbent, i.e., squeezing–vacuum drying for toxic expensive liquids and air drying for cheap volatile and innoxious liquids. The adsorption–desorption process was repeated five times. As shown in Fig. 8a, the poisonous methylbenzene was used as an example of squeezing–vacuum drying experiment. In the first cycle, 5.7 g of methylbenzene was adsorbed. But the mass of the adsorbed methylbenzene decreased to 5.1 g in the second cycle. From the second cycle onwards, the adsorption

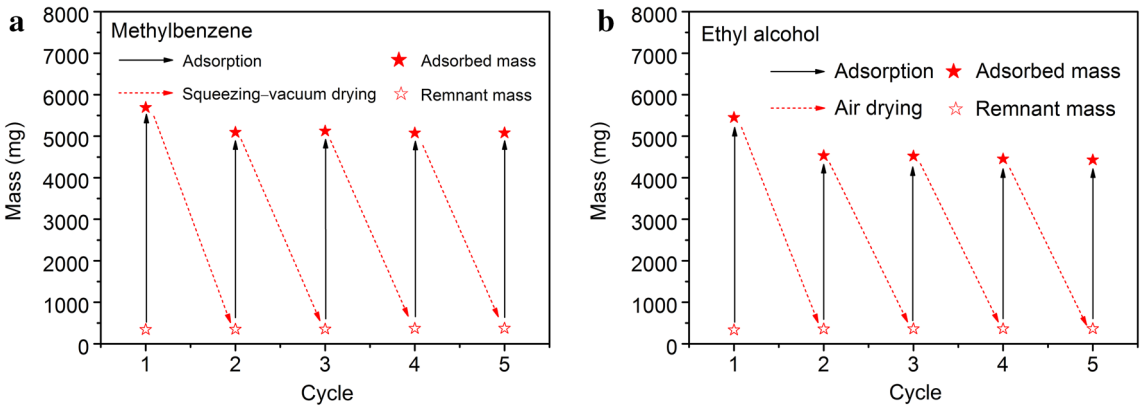

Fig. 8 Cyclic adsorption tests of the nonwoven cloth bag filled with the MTCS-treated NFC aerogels. **a** Squeezing–vacuum drying was used to recycle the adsorbent for adsorption of methylbenzene. **b** Air drying was applied to recycle the adsorbent for adsorption of ethyl alcohol

efficiency became stable, i.e., the weight increment kept constant (5.0–5.1 g). It can be seen that the adsorption efficiency maintained 88 % of the initial adsorption efficiency after the five cycles. As for the cyclic sorption–air drying test, the drying process was conducted in the fume hood at room temperature, and the next adsorption process did not begin until the sample weight maintained constant. It can be observed in Fig. 8b that the adsorbent still can adsorb 4.4 g ethyl alcohol after the five cycles, which is around 81 % of the first adsorption weight. Therefore, the two simple methods can be applied for recycling the adsorbent. Also, these results indicate that the adsorbent (i.e., the bag filled with the aerogels) has favorable adsorption recyclability.

4 Conclusions

We successfully used the waste natural reed to fabricate ultralight NFC aerogels via chemical purification, ultrasonication, and freeze drying. The FTIR analysis indicates the removal of non-cellulosic substances by the chemical purification. The SEM observation confirms that the NFCs with an average size of 22.67 nm were isolated. The XRD analysis demonstrates that the purification and ultrasonication did not change the cellulose crystal form (cellulose I). The NFC aerogels have a poorer thermal stability as a result of the ultrasonication, as compared to that of the reed and the purified cellulose. Through the hydrophobic modification by MTCS, the contact angles are as high as 151–155°. The adsorption efficiency of the hydrophobic aerogels reaches up to 53–93 g g^{-1} for various organic solvents and waste machine oil. For eliminating the effects of the poor mechanical property and strong shrinkage of the aerogels, we put the aerogels into a nonwoven cloth bag, and the bag was sealed and subjected to the cyclic adsorption tests. The two simple methods (i.e., squeezing–vacuum drying and air drying) can be applied for recycling the adsorbent dependent on the type of pollutants. The adsorbent can maintain more than 80 % of the initial adsorption efficiency after the five cycles. In summary, this work reports low-density superhydrophobic and high-performance adsorbents and provides an example to recycle waste bioresources and expands their high-value applications.

Acknowledgments This study was supported by the National Natural Science Foundation of China (Grant Nos. 31270590 and 31470584).

References

1. H.A. Khalil, A. Bhat, A.I. Yusra, Carbohyd. Polym. **87**, 963 (2012)
2. A. Kaushik, M. Singh, G. Verma, Carbohyd. Polym. **82**, 337 (2010)
3. L. Hu, G. Zheng, J. Yao, N. Liu, B. Weil, M. Eskilsson, E. Karabulut, Z. Ruan, S. Fan, J.T. Bloking, Energ. Environ. Sci. **6**, 513 (2013)
4. I. Siró, D. Plackett, Cellulose **17**, 459 (2010)
5. A. Liu, A. Walther, O. Ikkala, L. Belova, L.A. Berglund, Biomacromolecules **12**, 633 (2011)
6. S.-Y. Lee, S.-J. Chun, I.-A. Kang, J.-Y. Park, J. Ind. Eng. Chem. **15**, 50 (2009)
7. J. Zhao, W. Zhang, X. Zhang, X. Zhang, C. Lu, Y. Deng, Carbohyd. Polym. **97**, 695 (2013)
8. T. Isogai, T. Saito, A. Isogai, Cellulose **18**, 421 (2011)
9. W. Chen, H. Yu, Y. Liu, P. Chen, M. Zhang, Y. Hai, Carbohyd. Polym. **83**, 1804 (2011)
10. C. Wan, Y. Lu, Y. Jiao, C. Jin, Q. Sun, J. Li, J. Appl. Polym. Sci. **132**, 1 (2015)
11. B. Stefanovic, T. Rosenau, A. Potthast, Carbohyd. Polym. **92**, 921 (2013)
12. W. Li, J. Yue, S. Liu, Ultrason. Sonochem. **19**, 479 (2012)
13. A. Grönroos, P. Pirkonen, O. Ruppert, Ultrason. Sonochem. **11**, 9 (2004)
14. M. Tutt, J. Olt, Agron. Res. **9**, 261 (2011)
15. C. Somerville, S. Bauer, G. Brininstool, M. Facette, T. Hamann, J. Milne, E. Osborne, A. Paredez, S. Persson, T. Raab, Science **306**, 2206 (2004)

16. D.J. Cosgrove, Annu. Rev. Cell Dev. Bi. **13**, 171 (1997)
17. N. Mosier, C. Wyman, B. Dale, R. Elander, Y. Lee, M. Holtzapple, M. Ladisch, Bioresour. Technol. **96**, 673 (2005)
18. S. Zhu, Y. Wu, Z. Yu, C. Wang, F. Yu, S. Jin, Y. Ding, R.A. Chi, J. Liao, Y. Zhang, Biosyst. Eng. **93**, 279 (2006)
19. M. Pääkkö, J. Vapaavuori, R. Silvennoinen, H. Kosonen, M. Ankerfors, T. Lindström, L.A. Berglund, O. Ikkala, Soft Matter **4**, 2492 (2008)
20. H. Sehaqui, Q. Zhou, L.A. Berglund, Compos. Sci. Technol. **71**, 1593 (2011)
21. N.T. Cervin, C. Aulin, P.T. Larsson, L. Wågberg, Cellulose **19**, 401 (2012)
22. R. Xiong, C. Lu, Y. Wang, Z. Zhou, X. Zhang, J. Mater. Chem. A **1**, 14910 (2013)
23. D.O. Carlsson, G. Nyström, Q. Zhou, L.A. Berglund, L. Nyholm, M. Strømme, J. Mater. Chem. **22**, 19014 (2012)
24. C. Gebald, J.A. Wurzbacher, P. Tingaut, T. Zimmermann, A. Steinfeld, Environ. Sci. Technol. **45**, 9101 (2011)
25. H. Liu, W. Sha, A.T. Cooper, M. Fan, Coll. Surfare A **347**, 38 (2009)
26. A.V. Rao, N.D. Hegde, H. Hirashima, J. Coll. Interf. Sci. **305**, 124 (2007)
27. Z.-Y. Wu, C. Li, H.-W. Liang, Y.-N. Zhang, X. Wang, J.-F. Chen, S.-H. Yu, Sci. Rep-UK **4079**, 4 (2014)
28. H.W. Liang, Q.F. Guan, L.F. Chen, Z. Zhu, W.J. Zhang, S.H. Yu, Angew. Chem. Int. Edit. **51**, 5101 (2012)
29. H. Sun, Z. Xu, C. Gao, Adv. Mater. **25**, 2554 (2013)
30. F. Carrasco-Marín, D. Fairén-Jiménez, C. Moreno-Castilla, Carbon **47**, 463 (2009)
31. C. Wan, J. Li, Carbohyd. Polym. **134**, 144 (2015)
32. Y. Jiao, C. Wan, J. Li, Appl. Phys. A-Mater **120**, 341 (2015)
33. S. Boufi, A. Gandini, RSC Adv. **5**, 3141 (2015)
34. W. Chen, H. Yu, Y. Liu, Y. Hai, M. Zhang, P. Chen, Cellulose **18**, 433 (2011)
35. H. Wang, D. Li, R. Zhang, BioResources **8**, 1374 (2013)
36. E. Qua, P. Hornsby, H. Sharma, G. Lyons, R. McCall, J. Appl. Polym. Sci. **113**, 2238 (2009)
37. Z. Gao, M. Ma, X. Zhai, M. Zhang, D. Zang, C. Wang, RSC Adv. **5**, 63978 (2015)
38. R. Sun, S. Hughes, Carbohyd. Polym. **36**, 293 (1998)
39. O. Faix, O. Beinhoff, J. Wood Chem. Technol. **8**, 505 (1988)
40. Y. Lu, Q. Sun, D. Yang, X. She, X. Yao, G. Zhu, Y. Liu, H. Zhao, J. Li, J. Mater. Chem. **22**, 13548 (2012)
41. N. Abidi, L. Cabrales, C.H. Haigler, Carbohyd. Polym. **100**, 9 (2014)
42. C. Wan, Y. Lu, Q. Sun, J. Li, Appl. Surf. Sci. **321**, 38 (2014)
43. C. Wan, Y. Jiao, J. Li, Appl. Surf. Sci. **347**, 891 (2015)
44. H. Yang, R. Yan, H. Chen, D.H. Lee, C. Zheng, Fuel **86**, 1781 (2007)
45. A. Alves, M. Schwanninger, H. Pereira, J. Rodrigues, J. Anal. Appl. Pyrol. **76**, 209 (2006)
46. R. Capart, L. Khezami, A.K. Burnham, Thermochim. Acta **417**, 79 (2004)
47. S. Li, J. Lyons-Hart, J. Banyasz, K. Shafer, Fuel **80**, 1809 (2001)
48. S. Wang, X. Guo, K. Wang, Z. Luo, J. Anal. Appl. Pyrol. **91**, 183 (2011)
49. V. Alvarez, A. Vázquez, Polym. Degrad. Stabil. **84**, 13 (2004)
50. P. Lu, Y.-L. Hsieh, Carbohyd. Polym. **82**, 329 (2010)
51. W. Chen, H. Yu, Q. Li, Y. Liu, J. Li, Soft Matter **7**, 10360 (2011)
52. C. Aulin, J. Netrval, L. Wågberg, T. Lindström, Soft Matter **6**, 3298 (2010)
53. T.C.F. Silva, Y. Habibi, J.L. Colodette, T. Elder, L.A. Lucia, Cellulose **19**, 1945 (2012)
54. S. Hoepfner, L. Ratke, B. Milow, Cellulose **15**, 121 (2008)
55. F. Liebner, E. Haimer, M. Wendland, M.A. Neouze, K. Schlufter, P. Miethe, T. Heinze, A. Potthast, T. Rosenau, Macromol. Biosci. **10**, 349 (2010)
56. M. Shateri-Khalilabad, M.E. Yazdanshenas, Cellulose **20**, 3039 (2013)
57. Z. Zhang, G. Sèbe, D. Rentsch, T. Zimmermann, P. Tingaut, Chem. Mater. **26**, 2659 (2014)
58. A. Mulyadi, Z. Zhang, Y. Deng, A.C.S. Appl, Mater. Interfac **8**, 2732 (2016)
59. F. Jiang, Y.-L. Hsieh, J. Mater. Chem. A **2**, 6337 (2014)